


Graphene nanoribbons on hexagonal boron nitride: Deposition and transport characterization

Cite as: Appl. Phys. Lett. **114**, 173101 (2019); <https://doi.org/10.1063/1.5065568>

Submitted: 11 October 2018 . Accepted: 12 April 2019 . Published Online: 30 April 2019

Tobias Preis, Christian Kick, Andreas Lex, Dieter Weiss, Jonathan Eroms , Akimitsu Narita , Yunbin Hu , Klaus Müllen , Kenji Watanabe , and Takashi Taniguchi



View Online



Export Citation



CrossMark

ARTICLES YOU MAY BE INTERESTED IN

[Improved carrier doping strategy of monolayer MoS₂ through two-dimensional solid electrolyte of YBr₃](#)

Applied Physics Letters **114**, 171601 (2019); <https://doi.org/10.1063/1.5093712>

[Acoustically modulated optical emission of hexagonal boron nitride layers](#)

Applied Physics Letters **114**, 171104 (2019); <https://doi.org/10.1063/1.5093299>

[High-temperature electronic devices enabled by hBN-encapsulated graphene](#)

Applied Physics Letters **114**, 123104 (2019); <https://doi.org/10.1063/1.5088587>



Lake Shore
CRYOTRONICS

8600 Series VSM

For fast, highly sensitive measurement performance

[LEARN MORE](#) 

2017
**R&D
100
WINNER**

Graphene nanoribbons on hexagonal boron nitride: Deposition and transport characterization

Cite as: Appl. Phys. Lett. **114**, 173101 (2019); doi: [10.1063/1.5065568](https://doi.org/10.1063/1.5065568)

Submitted: 11 October 2018 · Accepted: 12 April 2019 ·

Published Online: 30 April 2019



View Online



Export Citation



CrossMark

Tobias Preis,¹ Christian Kick,¹ Andreas Lex,¹ Dieter Weiss,¹ Jonathan Eroms,^{1,a)}  Akimitsu Narita,² 
Yunbin Hu,^{2,b)}  Klaus Müllen,²  Kenji Watanabe,³  and Takashi Taniguchi³

AFFILIATIONS

¹Institute of Experimental and Applied Physics, University of Regensburg, D-93040 Regensburg, Germany

²Max Planck Institute for Polymer Research, Ackermannweg 10, D-55128 Mainz, Germany

³National Institute for Materials Science, 1-1 Namiki, Tsukuba 305-0044, Japan

^{a)}Electronic mail: jonathan.eroms@ur.de

^{b)}Present address: Department of Organic and Polymer Chemistry, College of Chemistry and Chemical Engineering, Central South University, Changsha, Hunan 410083, China.

ABSTRACT

Chemically synthesized “cove”-type graphene nanoribbons (cGNRs) of different widths were brought into dispersion and drop-cast onto exfoliated hexagonal boron nitride (hBN) on a Si/SiO₂ chip. Using AFM, we observed that the cGNRs form ordered domains aligned along the crystallographic axes of the hBN. Using electron beam lithography and metallization, we contacted the cGNRs with NiCr/Au or Pd contacts and measured their *I*-*V* characteristics. The transport through the ribbons was dominated by the Schottky behavior of the contacts between the metal and the ribbon.

Published under license by AIP Publishing. <https://doi.org/10.1063/1.5065568>

Confining graphene in one dimension yields graphene nanoribbons (GNRs), which have great potential for application in semiconductor technology. Depending on their width and edge configuration, GNRs can have a bandgap that, e.g., allows turning on and off the current flow in the GNR which is needed to design transistors.^{1–3} Initially, GNRs were obtained by top-down methods like etching structured graphene sheets³ or unzipping carbon nanotubes.^{4,5} However, these ribbons had rough edges which limit carrier transport and thus the usability of the GNRs in devices.^{6,7} Epitaxially grown GNRs on SiC show ballistic transport,⁸ and GNRs were prepared inside etched trenches in hexagonal boron nitride (hBN),⁹ but both the methods again lack atomic precision. Advances in solution chemistry opened up new routes to obtain GNRs by atomically precise bottom-up synthesis. There, GNRs are obtained by reactions of precursor molecules on catalytic metal surfaces.¹⁰ However, it is not possible to measure the GNRs' transport properties on a metal surface. One way to overcome this issue is to transfer the GNRs to insulating substrates (typically Si/SiO₂).^{11–13} The disadvantage here is that the transfer process usually involves etchants that contaminate the GNRs. Instead, solution-processable GNRs can be employed.^{14–17} Here, GNR powder is dispersed in a solvent and then drop-cast onto an arbitrary surface. In previous experiments, SiO₂ substrates were used, whose rough surface and charged impurities negatively influence carrier

transport. The mobility of extended graphene was shown to increase considerably when graphene was placed onto hexagonal boron nitride (hBN) instead of Si/SiO₂.¹⁸ For etched GNRs on hBN, on the other hand, sample properties did not improve due to disorder introduced by plasma etching.¹⁹ However, deposition and device fabrication of bottom-up-synthesized GNRs on hBN have not been reported. In this work, we demonstrate the deposition of GNRs onto the atomically flat surface of exfoliated hBN, showing a unique self-assembly behavior with domains of parallel aligned GNRs over tens to hundreds of nanometers. We further discuss the fabrication and characteristics of GNR-based FET devices on hBN.

We investigated solution-processable “cove”-type GNRs (cGNRs) of different widths^{14,20} [4 and 6 carbon dimers, see Figs. 1(a) and 1(b)]. These cGNRs were predicted to have a bandgap between 1.5 eV and 2.0 eV.^{21,22} The alkyl-side chains, which are attached for better solubility, were shown to have no substantial effect on the electronic structure.²³ To fabricate devices, cGNR powder (see our previous reports for the syntheses of the 4-cGNRs¹⁴ and 6-cGNRs²⁰) was put in tetrahydrofuran (THF) for the 4-cGNRs or in chlorobenzene for the 6-cGNRs, respectively. Hereafter, the mixture was sonicated for at least 1 h, until the powder was mostly dispersed and the dispersion turned violet (gray) for the 4-cGNRs (6-cGNRs), as can be seen in Fig. 1(c).

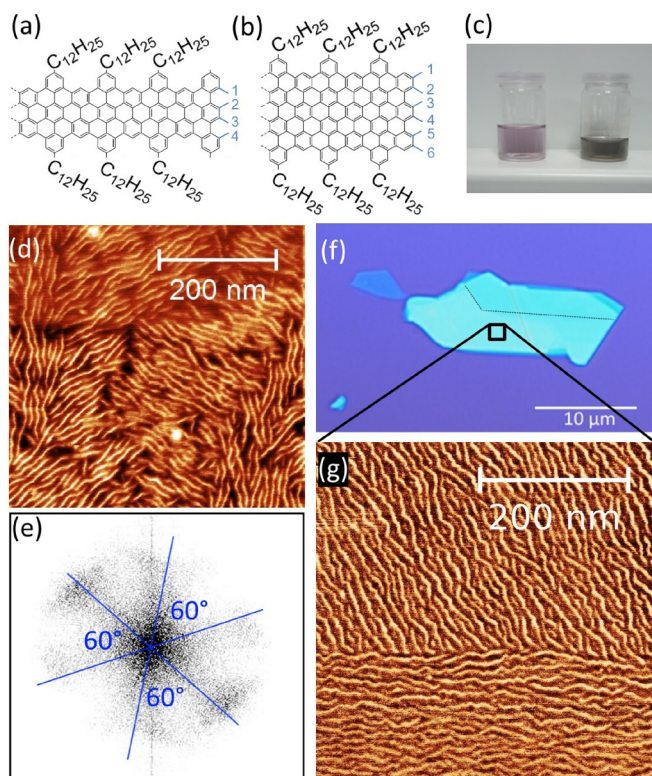


FIG. 1. cGNRs on hBN. (a) and (b) Chemical structure of 4- and 6-cGNRs. (c) Dispersion obtained after sonicating cGNR powder in THF (4-cGNR, left) and chlorobenzene (6-cGNR, right). (d) AFM phase image of 4-cGNRs on hBN. (e) 2D-FFT of (d) showing the preferential directions of the cGNRs. (f) Optical microscopy image of an exfoliated hBN flake on Si/SiO₂. (g) AFM phase image of 6-cGNRs [indicated area in (f)].

Subsequently, we exfoliated hBN on a Si/SiO₂ chip, drop-cast the cGNR dispersion onto the chip, and evaporated the solvent by placing the chip onto a hot plate. Afterwards, we investigated the flakes using an atomic force microscope (AFM). Figures 1(d) and 1(h) show AFM phase images of 4- and 6-cGNRs, respectively, on hBN flakes. In previous studies on SiO₂, it was found that cGNRs only adsorb on carefully functionalized substrates.^{15,16} Similarly, we did not observe cGNR adsorption on the untreated SiO₂ surface of our samples. In contrast, we found that cGNRs adsorb readily onto the atomically flat hBN surfaces and form well-ordered domains with domain sizes ranging from 60 nm to over 1 μm and ribbon lengths of up to 350 nm. Length distributions for both cGNR types can be found in the [supplementary material](#). The situation is similar to adsorption on highly oriented pyrolytic graphite (HOPG) surfaces,¹⁴ but with an important difference. While cGNRs on HOPG form arrays of straight ribbons, here we find that individual GNRs have a wiggled structure. Although we cannot offer a clear explanation for this observation, a possible reason could be the slight lattice mismatch between hBN and the graphene backbone of the cGNRs. This was shown in molecular dynamics simulations to lead to lateral buckling and snake-like motion of GNRs.²⁴ Alternatively, nonplanar adsorption of the alkyl-side chains on the hBN could play a role. It should be further

mentioned that the cGNRs seem to be very mobile on the hBN surface. cGNR covered hBN flakes were annealed to 450 °C and then reinvestigated using AFM. Before the annealing, the hBN flake was homogeneously covered with cGNRs, and after the annealing, the cGNRs seem to have formed agglomerates (see [supplementary material](#)) and the bare hBN flake is visible again. The superlubricity of armchair GNRs on a gold substrate was already reported in UHV experiments.²⁵ Finally, we note that, although we assume that the cGNRs form monolayers on the hBN flakes, given the z-resolution of our AFM, we cannot rule out that more than one layer of cGNRs is adsorbed on the hBN. The ordered domains of cGNRs on hBN are found to be rotated by 60° with respect to each other. The angles between the domains become especially clear when we plot a two-dimensional Fast Fourier Transformation (2D-FFT) of the AFM phase image [Fig. 1(e)]. The broadening of the 2D-FFT is mainly due to the wiggled structure of the cGNRs.

Figure 1(f) shows an optical microscopy image of an exfoliated hBN flake on a Si/SiO₂ chip before deposition of 6-cGNRs. When exfoliating hBN onto SiO₂, it often cleaves along its crystallographic axes. Consider the hexagonal lattice structure of hBN consisting of alternating B and N atoms,²⁶ which yields cleaving angles in multiples of 30°. Two of those axes are indicated with black dashed lines in Fig. 1(f). Figure 1(g) shows an AFM phase image of the area enclosed by the black square in Fig. 1(f) after drop-casting the 6-cGNRs onto the chip. When comparing the orientation of the cGNRs in Fig. 1(g) and the edges of the hBN flake in Fig. 1(f), it becomes apparent that the cGNR domains are aligned along the crystallographic axes of the hBN.

Next, we contacted the cGNRs by performing electron beam lithography and evaporating metals (thermally and e-beam). NiCr/Au or Pd²⁷ served as contact materials. Pd was deposited without any adhesion layer, and therefore, care had to be taken during lift-off not to damage the fine metal structures. We contacted multiple cGNRs at once, using interdigitated comb-like structures (see the lower inset of Fig. 2). The orientation of the contact combs was chosen in such a way that the contacts were perpendicular to some of the cGNR domains. Figure 2 shows an optical microscopy image of one device with 15 nm thick Pd contacts.

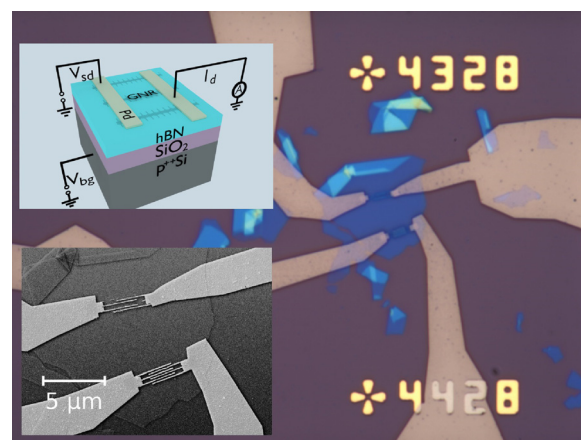


FIG. 2. Sample design. Optical microscopy image of an hBN flake on Si/SiO₂ with contacts reaching the cGNRs on the flake. (Distance between markers: 50 μm.) Lower inset: Magnified SEM image of the contact combs on the flake. Upper inset: Schematics of the measurement setup.

The schematics of the measurement setup is sketched in the upper inset of Fig. 2. With a probe station at ambient conditions, a source drain voltage V_{sd} was applied across the ribbons and the drain current I_d was measured. The heavily p-doped Si substrate could be used as a back gate electrode by applying a back gate voltage V_{bg} . The SiO_2 layer was 285 nm thick, and the thickness of the used hBN flakes varied between 10 and 40 nm and the spacing of the contacts between 70 and 120 nm.

Figure 3 shows I - V -measurements of 4- and 6-cGNRs contacted with NiCr/Au and Pd. The NiCr/Au contacted 4-cGNRs (black squares) show a current onset for the lowest source drain voltages. We note that all curves are asymmetric with respect to $V_{sd} = 0$. Possible sources for this asymmetry could be slightly different work functions of the electrodes due to contamination,²⁸ different contact areas,²⁹ or the fact that the bias voltage is not applied symmetrically, but with one terminal grounded.³⁰

The Pd contacted 4- and 6-cGNRs look very similar on the negative voltage side and differ only slightly on the positive side. This is quite surprising since their different bandgap should be reflected in the I - V -curves. Here, we assume that the Fermi level is always situated in the gap, as the curves can be described by a Schottky characteristic (see below). Further, when measuring contact pairs of further devices (of the same kind of cGNR and the same contact metal), the shape of the I - V -curves deviated from the curves shown in Fig. 3 and also the drain currents varied even by orders of magnitudes (see, e.g., the inset of Fig. 4). Taking all these effects into account, it seems likely that the measurements are dominated by the Schottky behavior of the contacts between the semiconducting cGNRs and the metallic electrodes. The transition from the metal to the cGNR and back to the metal can be seen as two back-to-back connected Schottky diodes^{31,32} with a resistor (one or many cGNRs) in-between (see the inset of Fig. 3). Since the detected current is limited by the current leaking through the Schottky diode in the reverse direction, we fitted the Schottky barriers separately for negative and positive voltage regions (for the reverse direction of the Schottky diode). The slight difference in the barrier height for positive and negative bias was included in the error margin. We found that the current density J of our data is best described by the thermionic field emission model^{28,29,33,34}

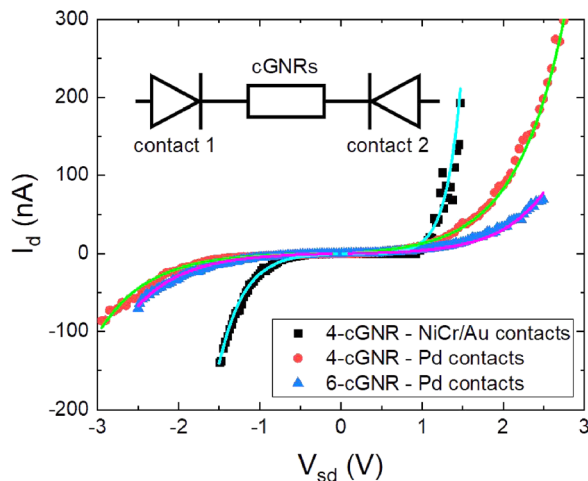


FIG. 3. I - V -curves. I - V -measurements of 4- and 6-cGNRs contacted with NiCr/Au and Pd (dots) and fits for the negative and positive voltage regions (lines). Inset: Schematics for two Schottky contacts connected back-to-back over a cGNR.

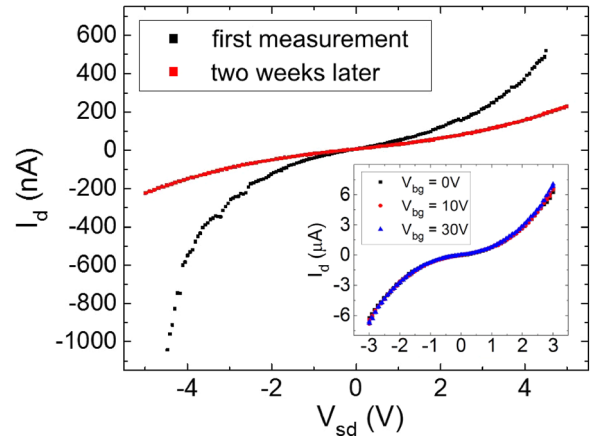


FIG. 4. Further measurements of 6-cGNRs. I - V -curves have been taken directly after device fabrication and two weeks later. The inset shows I - V -curves of a different sample at various back gate voltages.

$$J = \frac{AT\sqrt{\pi q E_{00}}}{k} \exp\left(-\frac{\Phi}{qE_0}\right) \exp\left[V\left(\frac{q}{kT} - \frac{1}{E_0}\right)\right] \times \sqrt{q(V - \zeta) + \frac{\Phi}{\cosh^2(qE_{00}/kT)}}. \quad (1)$$

Here, A is the Richardson constant, T the temperature, Φ the height of the Schottky barrier, k the Boltzmann constant, q the elementary charge, $V > 0$ the voltage applied across the barrier, and ζ the distance between the band edge and the Fermi level. E_{00} describes the shape of the barrier,³³ and $E_0 = E_{00} \coth(qE_{00}/kT)$. For the contact area, we take the cross-sectional area of one nanoribbon, but include the unknown number of parallel ribbons and further sources of uncertainty, in the error margin of Φ (for more details, see [supplementary material](#)). The fitting results are summarized in Table I. NiCr/Au yields a higher barrier than the Pd contacts. Furthermore, Pd contacts worked more reliably than NiCr/Au contacts which is why no data are shown for NiCr/Au contacted 6-cGNRs. Taking these facts into account, Pd seems to be the better contact material. The above numbers, however, have to be considered with care. Strictly speaking, the Richardson constant A is only valid for the free electron mass, but has to be modified using the electron effective mass,^{32,35} which is unknown for our contact configuration. We therefore used the free electron mass. Also, the alkyl-side chains could partially overlap with the cGNRs,¹⁴ leading to a further increase in the contact resistance. Both uncertainties are included in the error of the barrier height Φ . The obtained values of Φ are in line with earlier results on carbon nanotubes.³⁶

TABLE I. Fitting results for the graphs in Fig. 3.

Sample	Φ	E_{00}	ζ
NiCr/Au 4-cGNR	(190 ± 180) meV	16 mV	0.15 V
Pd 4-cGNR	(130 ± 180) meV	9 mV	0.2 V
Pd 6-cGNR	(150 ± 150) meV	9 mV	0.2 V

Additionally, we studied the stability of our fabricated devices in air. Figure 4 shows Pd contacted 6-cGNRs measured directly after fabrication (black squares) and two weeks later (red squares). The decreased drain current could be due to degradation of the cGNRs, degradation of the contacts, or contamination of the cGNRs by particles in the air.

Finally, we studied the gate response of our devices. As can be seen in the inset of Fig. 4, the devices showed (almost) no back gate dependence which could be due to Fermi level pinning at the Schottky contacts. Also, we note that the distance to the Si back gate is much larger than the separation of the metal electrodes. Therefore, we expect the gate coupling to be greatly reduced due to screening.

In previous studies, GNRs prepared from molecular precursors either by surface synthesis¹³ or in solution^{15,16} were deposited on oxidized silicon. When depositing 4-cGNRs dispersed in organic solvents or water onto SiO₂, careful surface functionalization was necessary.^{15,16,37} In this work, on the other hand, cGNRs adsorb readily onto the hBN surface. We found dense arrays of cGNRs on almost every hBN flake studied. This presents a clear advantage over the previous preparation method. In addition, hBN was shown to be a more suitable substrate for high-quality graphene devices. With respect to the contact transparency, we note that previous experiments on 4-cGNRs prepared from organic solvents and surface synthesized armchair GNRs found a device current in the 1 to 1000 nA range for a source drain bias of 1 V, in line with our observations.^{13,15,17} This also holds for 6-cGNRs which were not previously used in transport devices. In the case of cGNRs prepared from aqueous solution, Zschieschang *et al.* obtained a drain current of tens of microamperes. However, their devices showed signs of agglomeration, leading to a greatly reduced bandgap, which could explain the lower Schottky barrier.¹⁶

In summary, we dispersed chemically synthesized 4- and 6-cGNRs in THF or chlorobenzene. The dispersion was drop-cast onto exfoliated hBN. cGNRs adsorb readily onto the flat hBN surfaces and form ordered domains aligned along the crystallographic axes of the hBN, showing the potential of hBN as a substrate for GNR-based devices. We contacted the cGNRs with NiCr/Au or Pd contacts. The *I-V*-characteristics of the devices are dominated by the Schottky behavior of the contacts between the metal and the ribbon. Therefore, better contacts, such as edge-type contacts^{38–40} and local gates, are called for, which are technologically more demanding.

See [supplementary material](#) for an AFM image comparing the cGNR coverage on SiO₂ and hBN, for the effect of annealing, for the length distribution, for details on fitting the *I-V*-curves, and for an exemplary R_{sd} vs V_{bg} curve, showing no clear gate dependence.

Financial support by the Deutsche Forschungsgemeinschaft (DFG) within the programs SFB 689, GRK 1570, and SPP1459 and by the Max Planck Society for the synthesis of cGNRs is gratefully acknowledged. Growth of hexagonal boron nitride crystals was supported by the Elemental Strategy Initiative conducted by the MEXT, Japan, and JSPS KAKENHI Grant No. JP15K21722.

REFERENCES

- ¹F. Schwierz, *Nat. Nanotechnol.* **5**, 487 (2010).
- ²K. Nakada, M. Fujita, G. Dresselhaus, and M. S. Dresselhaus, *Phys. Rev. B* **54**, 17954 (1996).
- ³M. Y. Han, B. Özyilmaz, Y. Zhang, and P. Kim, *Phys. Rev. Lett.* **98**, 206805 (2007).
- ⁴D. V. Kosynkin, A. L. Higginbotham, A. Sinitskii, J. R. Lomeda, A. Dimiev, B. K. Price, and J. M. Tour, *Nature* **458**, 872 (2009).
- ⁵L. Jiao, L. Zhang, X. Wang, G. Diankov, and H. Dai, *Nature* **458**, 877 (2009).
- ⁶M. Y. Han, J. C. Brant, and P. Kim, *Phys. Rev. Lett.* **104**, 056801 (2010).
- ⁷M. Ewaldsson, I. V. Zozoulenko, H. Xu, and T. Heinzel, *Phys. Rev. B* **78**, 161407 (2008).
- ⁸J. Baringhaus, M. Ruan, F. Edler, A. Tejada, M. Sicot, A. Taleb-Ibrahimi, A.-P. Li, Z. Jiang, E. H. Conrad, C. Berger, C. Tegenkamp, and W. A. de Heer, *Nature* **506**, 349 (2014).
- ⁹L. Chen, L. He, H. S. Wang, H. Wang, S. Tang, C. Cong, H. Xie, L. Li, H. Xia, T. Li, T. Wu, D. Zhang, L. Deng, T. Yu, X. Xie, and M. Jiang, *Nat. Commun.* **8**, 14703 (2017).
- ¹⁰J. Cai, P. Ruffieux, R. Jaafar, M. Bieri, T. Braun, S. Blankenburg, M. Muoth, A. P. Seitsonen, M. Saleh, X. Feng, K. Müllen, and R. Fasel, *Nature* **466**, 470 (2010).
- ¹¹P. B. Bennett, Z. Pedramrazi, A. Madani, Y.-C. Chen, D. G. de Oteyza, C. Chen, F. R. Fischer, M. F. Crommie, and J. Bokor, *Appl. Phys. Lett.* **103**, 253114 (2013).
- ¹²Z. Chen, W. Zhang, C.-A. Palma, A. Lodi Rizzini, B. Liu, A. Abbas, N. Richter, L. Martini, X.-Y. Wang, N. Cavani, H. Lu, N. Mishra, C. Coletti, R. Berger, F. Klappenberger, M. Kläui, A. Candini, M. Affronte, C. Zhou, V. De Renzi, U. del Pennino, J. V. Barth, H. J. Räder, A. Narita, X. Feng, and K. Müllen, *J. Am. Chem. Soc.* **138**, 15488 (2016).
- ¹³J. P. Llinas, A. Fairbrother, G. Borin Barin, W. Shi, K. Lee, S. Wu, B. Yong Choi, R. Braganza, J. Lear, N. Kau, W. Choi, C. Chen, Z. Pedramrazi, T. Dumslaff, A. Narita, X. Feng, K. Müllen, F. Fischer, A. Zettl, P. Ruffieux, E. Yablonovitch, M. Crommie, R. Fasel, and J. Bokor, *Nat. Commun.* **8**, 633 (2017).
- ¹⁴A. Narita, X. Feng, Y. Hernandez, S. A. Jensen, M. Bonn, H. Yang, I. A. Verzhbitskiy, C. Casiraghi, M. R. Hansen, A. H. R. Koch, G. Fytas, O. Ivasenko, B. Li, K. S. Mali, T. Balandina, S. Mahesh, S. De Feyter, and K. Müllen, *Nat. Chem.* **6**, 126 (2014).
- ¹⁵A. N. Abbas, G. Liu, A. Narita, M. Orosco, X. Feng, K. Müllen, and C. Zhou, *J. Am. Chem. Soc.* **136**, 7555 (2014).
- ¹⁶U. Zschieschang, H. Klauk, I. B. Müller, A. J. Strudwick, T. Hintermann, M. G. Schwab, A. Narita, X. Feng, K. Müllen, and R. T. Weitz, *Adv. Electron. Mater.* **1**, 1400010 (2015).
- ¹⁷P. Fantuzzi, L. Martini, A. Candini, V. Corradini, U. del Pennino, Y. Hu, X. Feng, K. Müllen, A. Narita, and M. Affronte, *Carbon* **104**, 112 (2016).
- ¹⁸C. R. Dean, A. F. Young, I. Meric, C. Lee, L. Wang, S. Sorgenfrei, K. Watanabe, T. Taniguchi, P. Kim, K. L. Shepard, and J. Hone, *Nat. Nanotechnol.* **5**, 722 (2010).
- ¹⁹D. Bischoff, T. Krähenmann, S. Dröscher, M. A. Gruner, C. Barraud, T. Ihn, and K. Ensslin, *Appl. Phys. Lett.* **101**, 203103 (2012).
- ²⁰Y. Hu, P. Xie, M. De Corato, A. Ruini, S. Zhao, F. Meggendorfer, L. A. Straasø, L. Rondin, P. Simon, J. Li, J. J. Finley, M. R. Hansen, J.-S. Lauret, E. Molinari, X. Feng, J. V. Barth, C.-A. Palma, D. Prezzi, K. Müllen, and A. Narita, *J. Am. Chem. Soc.* **140**, 7803 (2018).
- ²¹S. Osella, A. Narita, M. G. Schwab, Y. Hernandez, X. Feng, K. Müllen, and D. Beljonne, *ACS Nano* **6**, 5539 (2012).
- ²²I. Ivanov, Y. Hu, S. Osella, U. Beser, H. I. Wang, D. Beljonne, A. Narita, K. Müllen, D. Turchinovich, and M. Bonn, *J. Am. Chem. Soc.* **139**, 7982 (2017).
- ²³C. E. P. Villegas, P. B. Mendonça, and A. R. Rocha, *Sci. Rep.* **4**, 6579 (2014).
- ²⁴W. Ouyang, D. Mandelli, M. Urbakh, and O. Hod, *Nano Lett.* **18**, 6009 (2018).
- ²⁵S. Kawai, A. Benassi, E. Gnecco, H. Söde, R. Pawlak, X. Feng, K. Müllen, D. Passerone, C. A. Pignedoli, P. Ruffieux, R. Fasel, and E. Meyer, *Science* **351**, 957 (2016).
- ²⁶T. Taniguchi and K. Watanabe, *J. Cryst. Growth* **303**, 525 (2007).
- ²⁷F. Xia, V. Perebeinos, Y.-m. Lin, Y. Wu, and P. Avouris, *Nat. Nanotechnol.* **6**, 179 (2011).
- ²⁸D. J. Perello, S. C. Lim, S. J. Chae, I. Lee, M. J. Kim, Y. H. Lee, and M. Yun, *ACS Nano* **5**, 1756 (2011).
- ²⁹Z. Zhang, K. Yao, Y. Liu, C. Jin, X. Liang, Q. Chen, and L.-M. Peng, *Adv. Funct. Mater.* **17**, 2478 (2007).
- ³⁰J. Appenzeller, J. Knoch, V. Derycke, R. Martel, S. Wind, and P. Avouris, *Phys. Rev. Lett.* **89**, 126801 (2002).

- ³¹A. J. Chiquito, C. A. Amorim, O. M. Berengue, L. S. Araujo, E. P. Bernardo, and E. R. Leite, *J. Phys.: Condens. Matter* **24**, 225303 (2012).
- ³²S. M. Sze and K. K. Ng, *Physics of Semiconductor Devices*, 3rd ed. (John Wiley & Sons, 2007).
- ³³F. A. Padovani and R. Stratton, *Solid-State Electron.* **9**, 695 (1966).
- ³⁴Y. Liu, Z. Y. Zhang, Y. F. Hu, C. H. Jin, and L.-M. Peng, *J. Nanosci. Nanotechnol.* **8**, 252 (2008).
- ³⁵C. Crowell, *Solid-State Electron.* **8**, 395 (1965).
- ³⁶J. Svensson and E. E. B. Campbell, *J. Appl. Phys.* **110**, 111101 (2011).
- ³⁷R. Konnerth, C. Cervetti, A. Narita, X. Feng, K. Müllen, A. Hoyer, M. Burghard, K. Kern, M. Dressel, and L. Bogani, *Nanoscale* **7**, 12807 (2015).
- ³⁸Y. Matsuda, W.-Q. Deng, and W. A. Goddard, *J. Phys. Chem. C* **114**, 17845 (2010).
- ³⁹L. Wang, I. Meric, P. Y. Huang, Q. Gao, Y. Gao, H. Tran, T. Taniguchi, K. Watanabe, L. M. Campos, D. A. Muller, J. Guo, P. Kim, J. Hone, K. L. Shepard, and C. R. Dean, *Science* **342**, 614 (2013).
- ⁴⁰J.-W. Huang, C. Pan, S. Tran, B. Cheng, K. Watanabe, T. Taniguchi, C. N. Lau, and M. Bockrath, *Nano Lett.* **15**, 6836 (2015).